University of Pennsylvania
ScholarlyCommons

Departmental Papers (MSE) Department of Materials Science & Engineering

November 2006

Applications of electron microscopy to the characterization of semiconductor nanowires

Douglas Tham
University of Pennsylvania

Chang-Yong Nam
University of Pennsylvania

Kumhyo Byon
University of Pennsylvania

Jinyong Kim
University of Pennsylvania

John E. Fischer
University of Pennsylvania, fischer@seas.upenn.edu

Follow this and additional works at: http://repository.upenn.edu/mse_papers

Recommended Citation

Tham, D., Nam, C., Byon, K., Kim, J., & Fischer, J. E. (2006). Applications of electron microscopy to the characterization of semiconductor nanowires. Retrieved from http://repository.upenn.edu/mse_papers/119

Postprint version. Published in *Applied Physics A: Materials Science & Processing*, Volume 85, Issue 3, November 2006, pages 227-231.
Publisher URL: http://dx.doi.org/10.1007/s00339-006-3705-y

This paper is posted at ScholarlyCommons. http://repository.upenn.edu/mse_papers/119
For more information, please contact libraryrepository@pobox.upenn.edu.

Applications of electron microscopy to the characterization of semiconductor nanowires

Abstract
We review our current progress on semiconductor nanowires of β-Ga_2O_3, Si and GaN. These nanowires were grown using both vapor–solid (VS) and vapor–liquid–solid (VLS) mechanisms. Using transmission electron microscopy (TEM) we studied their morphological, compositional and structural characteristics. Here we survey the general morphologies, growth directions and a variety of defect structures found in our samples. We also outline a method to determine the nanowire growth direction using TEM, and present an overview of device fabrication and assembly methods developed using these nanowires.

Comments
Postprint version. Published in *Applied Physics A: Materials Science & Processing*, Volume 85, Issue 3, November 2006, pages 227-231.
Publisher URL: http://dx.doi.org/10.1007/s00339-006-3705-y

This journal article is available at ScholarlyCommons: http://repository.upenn.edu/mse_papers/119

Applications of electron microscopy to the characterization of semiconductor nanowires

*Douglas Tham, Chang-Yong Nam, Kumhyo Byon, Jinyong Kim, John E. Fischer**

Department of Materials Science and Engineering
University of Pennsylvania
3231 Walnut Street, Philadelphia PA 19104-6272 (USA)

(*Corresponding author email: fischer@seas.upenn.edu)

PACS numbers: 61.14.-x, 81.07.-b, 61.14.-Lj, 81.05.-t

Abstract

We review our current progress on semiconductor nanowires of β-Ga_2O_3, Si and GaN. These nanowires were grown using both vapor-solid (VS) and vapor-liquid-solid (VLS) mechanisms. Using transmission electron microscopy (TEM) we studied their morphological, compositional and structural characteristics. Here we survey the general morphologies, growth directions and a variety of defect structures found in our samples. We also outline a method to determine the nanowire growth direction using TEM, and present an overview of device fabrication and assembly methods developed using these nanowires.

1. Introduction

In recent years semiconductor nanowires have emerged as promising functional materials readily amenable to integration into future solid state devices, and as such they have been intensely studied [1-5]. In particular, nanowires combine the high surface area typical of nanostructures with a rod-like geometry intuitively suitable for electronic and optoelectronic applications [6-11]. In sufficiently thin nanowires, two-dimensional quantum confinement effects can be observed, although weaker than in quantum dots due to the loss of a confinement dimension [12]. Nonetheless, the list of potential applications appears only to be limited by the imagination and by the quality of the material. Consequently, the synthesis, characterization and assembly of nanowires (and related nanostructures) has become a rich field of research.

Transmission electron microscopy (TEM) is a well-established analytical technique used in many nanowire characterization studies [13-17]. There is arguably no other technique capable of imaging internal defect structures at near-atomic resolution. Furthermore, the TEM is extremely versatile, combining within a single instrument the complementary capabilities of imaging, diffraction and spectroscopy, all at exceptionally high spatial resolution. These can often be executed nearly simultaneously on the same region of interest, providing a wealth of morphological, structural and compositional information required to solve cutting-edge materials science problems.

In this paper, we review our work on semiconductor nanowires and give a broad overview of the synthetic approaches and experimental techniques developed over 4 years of intense work. Key findings are summarized and the most important and representative results from TEM results are highlighted. First we describe the synthetic techniques and the sometimes bewildering variety of morphological characteristics observed. Then we present a general method for determining the crystallographic orientation of nanowire axes, along with some examples. There follows an examination of common types of defects resulting from our growth methods. We conclude with a brief summary of recent progress in device fabrication and assembly.

2. Nanowire Synthesis

We have explored two main approaches to the growth of semiconductor nanowires. The vapor-solid (VS) growth mechanism avoids the use of catalysts. Using a horizontal tube furnace, a source pellet or powder is heated to 1100°C or greater to vaporize the source material, while a controlled mixture of inert and/or reactive gas flows through the furnace tube. A Si wafer chip is placed downstream of the source, and nanostructures grow directly on the chip surface which is maintained ~100-500°C cooler than the source. With calibrated temperature gradient, several substrates located at different temperatures can be processed simultaneously. Crystalline nanostructures generally grow along fast growth directions, such that when the growth rate of a particular crystal structure are significantly higher along a particular crystal axis, then nanowires will result. The details of VS type growth are still not well understood; however under certain conditions epitaxial growth may also occur [18, 19]. Using this method we have successfully grown nanowires of β-Ga_2O_3 (unpublished), Si [20] and GaN [21].

The alternative approach uses metal catalysts (typically Au, AuPd or Pt in this work) to direct the growth of nanowires *via* the well-studied vapor-liquid-solid (VLS) mechanism [15, 16, 22]. Above the melting point the metal catalyst droplets dissolve precursor atoms from the vapor, nucleating nanowires when the solution becomes supersaturated. A key aspect of VLS growth is that the catalyst particles constrain the radial growth of nanowires and direct the growth along fast crystal growth directions. Provided that the particles are sufficiently small and are atop a suitable crystalline substrate, nanowires may grow epitaxially on the substrate [23-26]. Metal particles can be obtained by pre-heating a very thin sputtered film which breaks up into droplet islands upon heating, or by some form of patterned deposition [27]. We have employed the catalytic VLS to the growth of Si and GaN nanowires [28-31].

3. Morphologies

A broad range of nanostructure morphologies are accessible using the synthetic processes outlined above. Our β-Ga_2O_3 nanostructures grown *via* the VS mechanism exhibit a great variety of forms (see Fig. 1), as also reported by other researchers [32-34]. These include one-dimensional nanowires, two-dimensional structures such as nanobelts and nanosheets (Fig. 1a), and even dendritic structures we refer to as “nanotrees” (Fig.

1b). Another example of morphology diversity is found in VS-grown GaN nanostructures, where we observe a broad variety of forms ranging from nanowires to nanobelts to polyhedral crystals, depending on the growth conditions [21].

Similarly, VS-grown Si nanostructures exhibit two common morphologies. The first is the familiar "core-shell" nanowire, with a cylindrical Si core surrounded by an amorphous SiO_x sheath. The second is the "nanochain" morphology, wherein beads of Si nanocrystals passivated by a thin surface oxide are connected by fine amorphous silica nanowires to other Si nanocrystals, much like a string-of-pearls. While VS growth models for nanowire formation have been proposed [35], the mechanism for nanochain formation remains poorly studied; one speculation is that impurity incorporation at the beads plays an important role [36]. Both types of Si nanostructures are seen in the TEM micrograph in Fig. 2. The morphological details of each nanostructure can be appreciated from the insets, chemical maps for crystalline Si and amorphous SiO_2 obtained using energy-filtered TEM (EFTEM) [20]. These clearly reveal that the nanowire in the upper left corner is in fact a Si/SiO_x core-sheath structure, in contrast to the nanochain (center left) is primarily SiO_x . Coiled structures are occasionally observed; these too are primarily SiO_x with no clear evidence for a "pure" Si core.

Clean nanowire morphology almost invariably results when VLS catalysts are used. At the end of a growth run, metal catalyst spheres are found segregated onto the free ends of the wires. This always occurs in the case of GaN with AuPd catalyst, Fig. 3a). Energy-dispersive x-ray spectra (XEDS, Fig. 3b) and electron energy loss spectra (EELS, not shown) confirm that incorporation AuPd into the nanowire is below the detection limit of either method.

4. Growth Directions

Nanowire growth directions are generally determined using the TEM, either from lattice fringe spacings or selected area electron diffraction (SAED). After the required calibrations are performed, a micrograph and a diffraction pattern can be obtained from the same nanowire. The pair of images is compared to identify the row of diffraction

spots that run parallel to the nanowire axis and pass through the 000 spot. *Assuming that the nanowire is orthogonal to the electron beam*, these spots arise from lattice planes perpendicular to the nanowire axis. The problem then becomes a matter of working out the crystallographic growth direction.

However, using TEM to determine the nanowire growth direction is not straightforward because the image is a projection of a three-dimensional specimen that is in general tilted with respect to the electron beam. This tilt cannot be easily determined except in special cases with a rigid specimen where its orientation is related specifically to its microstructure. Therefore, it is unsatisfactory to assume that nanowires are orthogonal to the electron beam, because differences in tilt can arise easily from bent or broken areas of the TEM support film, from non-rigid nanowires, and obviously from tilting of the sample stage initiated by the operator.

Diffraction spots arise from those lattice planes that satisfy the Bragg diffraction condition. Conceivably, there can be a large set of lattice planes (generally oblique to the nanowire axis) that satisfy the Bragg condition as the nanowire is tilted. If the nanowire is not orthogonal to the electron beam, the diffraction spots used to determine the growth direction can arise from any of these oblique lattice planes. The result is that the growth direction is determined incorrectly. As it turns out, a single diffraction pattern provides insufficient information to determine the nanowire growth direction.

To address this problem, we developed a two-tilt diffraction technique to unequivocally determine the growth directions of Ga_2O_3, Si and GaN nanowires [37]. The method is based on the fact that two different planes parallel to a cylinder must intersect along a line parallel to the cylinder axis. If the plane normals to these two planes are known, then the cross product of the plane normal vectors provides the desired axis direction.[*] In practice, a plane parallel to the nanowire axis is identified and indexed using electron diffraction (i.e., its diffraction spots are *perpendicular* to the nanowire

[*] Given two plane normals $\mathbf{n}_1$ and $\mathbf{n}_2$ in Miller indices $\{h_1k_1l_1\}$ and $\{h_2k_2l_2\}$, plane normals in reciprocal lattice vectors $\mathbf{a}^*$, $\mathbf{b}^*$, $\mathbf{c}^*$ can be written as $\mathbf{n}_1 = h_1\mathbf{a}^* + k_1\mathbf{b}^* + l_1\mathbf{c}^*$ and $\mathbf{n}_2 = h_2\mathbf{a}^* + k_2\mathbf{b}^* + l_2\mathbf{c}^*$. If these two plane normals are crossed, the line of intersection $\mathbf{r}$ is $\mathbf{r} = \mathbf{n}_1 \times \mathbf{n}_2 = (h_1\mathbf{a}^* + k_1\mathbf{b}^* + l_1\mathbf{c}^*) \times (h_2\mathbf{a}^* + k_2\mathbf{b}^* + l_2\mathbf{c}^*) = u\mathbf{a} + v\mathbf{b} + w\mathbf{c}$, using the identities $\mathbf{a} = \mathbf{b}^* \times \mathbf{c}^*$ etc. The index $[uvw]$ of the line of intersection between the two planes is equal to the cross product of the two plane indices.

axis). Then the sample is tilted to a new zone axis and the process repeated. The growth direction is obtained from the cross product of the Miller indices of these two planes.

This technique is particularly useful for low symmetry crystals such as β-Ga_2O_3. In fact this was the only way to obtain the correct growth direction for wires comprising the β-Ga_2O_3 “nanotrees”, because these wires were self-supported at oblique angles to the electron beam. Two of the fast crystal growth directions were <010> and <001>, and many nanowires grew along these directions. Figure 4 shows an example of a β-Ga_2O_3 nanowire grown along <001>. These are also the growth directions commonly reported in the literature for β-Ga_2O_3 nanowires and nanobelts [37-39], so we are confident that our technique is robust.

Our VS-grown Si nanowires [20] were mostly grown along the commonly reported <111> and <211> directions [25, 35, 36]. Figure 5a shows a typical VS-grown Si nanowire, with a ~15 nm diameter crystalline Si core sheathed with ~10 nm of amorphous oxide. Figure 5b is the associated convergent beam electron diffraction (CBED) pattern of this Si nanowire, showing that the growth direction is along <111>.

The VLS-grown GaN nanowires were mostly grown along <120>, and exhibited isosceles triangular cross-sections commonly reported in the literature [24, 40]. Figure 6a shows a typical VLS-grown GaN nanowire, grown along <120> via the stacking of (010) planes at the catalyst-nanowire interface (Fig. 6b). Additionally, we were able to determine the faceting relationship of the nanowires using CBED on a nanowire cross-section.[29] By matching experimental and simulated CBED patterns, we showed that these triangular nanowires were faceted to expose the (001), $(2\bar{1}\bar{2})$ and $(\bar{2}1\bar{2})$ surfaces.

5. Defects

Defects are difficult to avoid in our growth system, and we observe planar defects in all our samples. In VS-grown β-Ga_2O_3 nanowires, these appear to run parallel and oblique to the nanowire axes (note the oblique contrast variations near the tip of the nanowire in Fig. 4). Planar defects in β-Ga_2O_3 nanowires have been reported by other workers as well, but detailed characterization of these defects remains scarce [38, 41-43].

Planar defects are also common in our Si nanowires [20], and these are {111} type twins that run obliquely across the nanowire (see arrowed feature in Fig. 5a) but

never along the nanowires. The phenomenon of {111} twinning in Si nanowires, prepared using a method similar to ours, has already been studied closely in the literature [44]. The high incidence of twinning in Si nanowires appears to be unique to the "oxide-assisted" VS-growth system [35], since Si nanowires prepared using VLS catalyzed chemical vapor deposition (CVD) do not appear to contain these defects [11, 45]. Oxygen in the growth system may be responsible, since it is known that Czochralski-grown Si is vulnerable to oxygen-induced stacking faults [46].

In GaN nanowires, planar defects tend to run along the axis, and are usually (001) stacking faults or rotational twins about the growth axis [31]. The contrast variations across the nanowire in Figure 6 are due to (001) stacking faults, which can be seen to run along the entire length of the GaN nanowire right up to the catalyst-nanowire interface. To understand why these axial planar defects are so prevalent, we recently proposed a defect-mediated VLS growth model [31]. These defects expose higher-energy sites at the growth front that serve as nucleation centers, resulting in faster crystal growth rate. Therefore, with axial defects these nucleation sites persist throughout the nanowire growth stage, and result in a sustained increase in the growth rate. Similar effects may influence the kinetics of nanowire growth *via* the VS mechanism.

6. Device Fabrication and Assembly

We have fabricated single nanowire devices using dielectrophoretic assembly, lithographic contact patterning, and direct writing. We have successfully demonstrated that dielectrophoretic assembly is a viable technique to assemble β-Ga_2O_3 nanowire arrays (unpublished data). We used lithographic contact patterning to fashion Si nanowire FETs and were able to modulate the electrical characteristics of the fabricated Si nanowire FETs from *p*- to *n*-type via post-growth doping [20].

We have also been able to control the exact positions of nanowires grown on a substrate. Using the "direct writing" capability of a focused-ion-beam (FIB) instrument, we first deposited a pattern of nanometer-sized Pt catalyst islands on our growth substrates. After optimizing the Pt catalyst and growth parameters, well-isolated nanowires suitable for device fabrication were found growing from the Pt catalyst sites

[27]. No nanowires were found other than these, so under the growth conditions the Pt catalyst was a necessity (VLS growth).

We also showed that ion beam assisted deposition of Pt contacts from an organometallic precursor is an efficient approach to fabricating GaN nanowire circuits. FIB-Pt gives low resistance ohmic contacts to our *n*-type GaN nanowires [28]. Pt contacts on bulk *n*-GaN are usually rectifying, due to the formation of a Schottky barrier at the contact interface, but using cross-sectional TEM we found that FIB-induced damage to the nanowires [30] produced sufficient disorder for Mott variable range hopping to dominate the contact conduction in sufficiently small nanowires [28].

We also fabricated and studied electromechanical oscillators from GaN nanowires [29]. These exhibit resonant oscillations with high quality factors, which we attribute to the excellent surface quality of the GaN nanowires. In some cases we were able to detect two closely-spaced resonances consistent with the the low symmetry and highly perfect isosceles triangular cross-section. The Young's modulus, derived from resonant frequencies and nanowire dimensions, is comparable to the bulk value for large "diameter" wires, but decreases by 35% as d approaches 35 nm.

7. Conclusions

Our group has synthesized β-Ga_2O_3, Si and GaN nanowires using both VS and VLS type growth, and we have observed several commonly observed morphologies in our samples. Growth directions of these nanowires are not always straightforward to obtain, and we have outlined a general technique for measuring nanowire growth directions in the TEM. Using our technique we identified the common growth directions in our nanowires, and have begun to relate nanowire morphological features with the underlying crystal structure. In our growth system, we have not been able to avoid the formation of defects in our nanowires, and in fact we have observed planar defects in all our samples. Finally, we have successfully fabricated nanowire devices using a variety of assembly techniques and explored their device behavior.

Acknowledgements

This research was supported by the US Department of Energy Grant DE-FG02-98ER45701. The use of shared facilities supported by Penn's NSF/MRSEC under Grant DMR02-03378 is gratefully acknowledged.

References

1. M. Law, et al., *Annu. Rev. Mater. Res.*, ***34***, 83-122 (2004)

2. Y. Huang, C. M. Lieber, *Pure Applied Chemistry*, ***76***, 2051-2068 (2004)

3. P. Yang, *MRS Bull.*, ***30***, 85-91 (2005)

4. Z. L. Wang, *Adv. Mater.*, ***15***, 432-436 (2003)

5. A. Kolmakov, M. Moskovits, *Annu. Rev. Mater. Res.*, ***34***, 151-180 (2004)

6. H. Kind, et al., *Adv. Mater.*, ***14***, 158-160 (2002)

7. Y. Huang, et al., *Nano Lett.*, ***2***, 101-104 (2002)

8. F. Qian, et al., *Nano Lett.*, ***4***, 1975-1979 (2004)

9. Y. Zhang, et al., *Nano Lett.*, ***4***, 403-407 (2004)

10. M. T. Björk, et al., *Nano Lett.*, ***4***, 1621-1625 (2004)

11. G. Zheng, et al., *Adv. Mater.*, ***16***, 1890-1893 (2004)

12. H. Yu, et al., *Nature Mater.*, ***2***, 517-520 (2003)

13. D. C. Bell, et al., *Microsc. Res. Tech.*, ***64***, 373-389 (2004)

14. W. S. Shi, et al., *Chem. Phys. Lett.*, ***345***, 377-380 (2001)

15. E. A. Stach, et al., *Nano Lett.*, ***3***, 867-869 (2003)

16. Y. Wu, P. Yang, *J. Am. Chem. Soc.*, ***123***, 3165-3166 (2001)

17. Z. L. Wang, et al., *Microsc. Microanal.*, ***8***, 467-474 (2002)

18. J. Noborisaka, et al., *Appl. Phys. Lett.*, ***86***, 213102 (2005)

19. W. Lee, et al., *Acta Mater.*, ***52***, 3949-3957 (2004)

20. K. Byon, et al., *Appl. Phys. Lett.*, ***87***, 193104 (2005)

21. C. Y. Nam, et al., *Appl. Phys. Lett.*, ***85***, 5676-5678 (2004)

22. R. S. Wagner, W. C. Ellis, *Appl. Phys. Lett.*, ***4***, 89-90 (1964)

23. P. Nguyen, et al., *Nano Lett.*, ***3***, 925-928 (2003)

24. T. Kuykendall, et al., *Nature Mater.*, ***3***, (2004)

25. A. I. Hochbaum, et al., *Nano Lett.*, ***5***, 457-460 (2005)

26. T. Mårtensson, et al., *Nano Lett.*, ***4***, 1987-1990 (2004)

27. C. Y. Nam, et al., *Appl. Phys. Lett.*, ***86***, 193112 (2005)

28. C. Y. Nam, et al., *Nano Lett.*, ***5***, 2029-2033 (2005)

29. C. Y. Nam, et al., *Nano Lett.*, ***6***, 153-158 (2006)

30. D. Tham, et al., *Adv. Mater.*, ***18***, 290-294 (2006)

31. D. Tham, et al., *Adv. Funct. Mater.*, DOI: 10.1002/adfm.200500807 (2006)
32. Z. R. Dai, et al., *Adv. Funct. Mater.*, ***13***, 9-24 (2003)
33. G. Gundiah, et al., *Chem. Phys. Lett.*, ***351***, 189-194 (2002)
34. Z. L. Wang, *Annu. Rev. Phys. Chem.*, ***55***, 159-196 (2004)
35. R.-Q. Zhang, et al., *Adv. Mater.*, ***15***, 635-640 (2003)
36. R. J. Barsotti, Jr., et al., *Appl. Phys. Lett.*, ***81***, 2866-2868 (2002)
37. Z. R. Dai, et al., *J. Phys. Chem. B*, ***106***, 902-904 (2002)
38. L. Dai, et al., *J. Appl. Phys.*, ***92***, 1062-1064 (2002)
39. J. Q. Hu, et al., *J. Phys. Chem. B*, ***106***, 9536-9539 (2002)
40. T. Kuykendall, et al., *Nano Lett.*, ***3***, 1063-1066 (2003)
41. H. J. Chun, et al., *J. Phys. Chem. B*, ***107***, 9042-9046 (2003)
42. H. Z. Zhang, et al., *Solid State Commun.*, ***109***, 677-682 (1999)
43. G.-S. Park, et al., *J. Cryst. Growth*, ***220***, 494-500 (2000)
44. X. L. Ma, et al., *Philos. Mag. Lett.*, ***82***, 461-468 (2002)
45. S. Sharma, M. K. Sunkara, *Nanotechnol.*, ***15***, 130-134 (2004)
46. S. Wolf, *Microchip Manufacturing* (Lattice Press 1943)

Figure captions

Figure 1 – (a) Scanning electron micrograph of nanowires, nanobelts, and nanosheets of β-Ga_2O_3. (b) Scanning electron micrograph of β-Ga_2O_3 nanotrees.

Figure 2 – (a) EFTEM image of VS-grown Si nanowires and nanochains. Chemical maps show the distribution of (b) crystalline Si and (c) amorphous SiO_2 in these nanostructures.

Figure 3 – (a) TEM image of VLS-grown GaN nanowire, tipped with a dark AuPd catalyst particle. (b) X-ray energy dispersive spectra (XEDS) of catalyst tip and nanowire, showing that the catalyst is AuPd and the nanowire is GaN. Cu system peaks have not been labeled for clarity.

Figure 4 – TEM image of a VS-grown β-Ga_2O_3 nanowire grown along the <001> direction. (Inset) Selected area electron diffraction (SAED) pattern of the β-Ga_2O_3 nanowire.

Figure 5 – (a) TEM image of a VS-grown Si nanowire grown along the <111> direction. The large arrow indicates a stacking fault defect. (b) Convergent beam electron diffraction (CBED) pattern of the Si nanowire.

Figure 6 – (a) TEM image of a VLS-grown GaN nanowire grown along the <120> direction, tipped with an AuPd catalyst particle. The axial contrast striations within the nanowire are due to [001] stacking faults in the wurtzite GaN, creating small thin regions of cubic GaN and resulting in a layered appearance. (b) Convergent beam electron diffraction (CBED) pattern of the GaN nanowire.

Figure 1

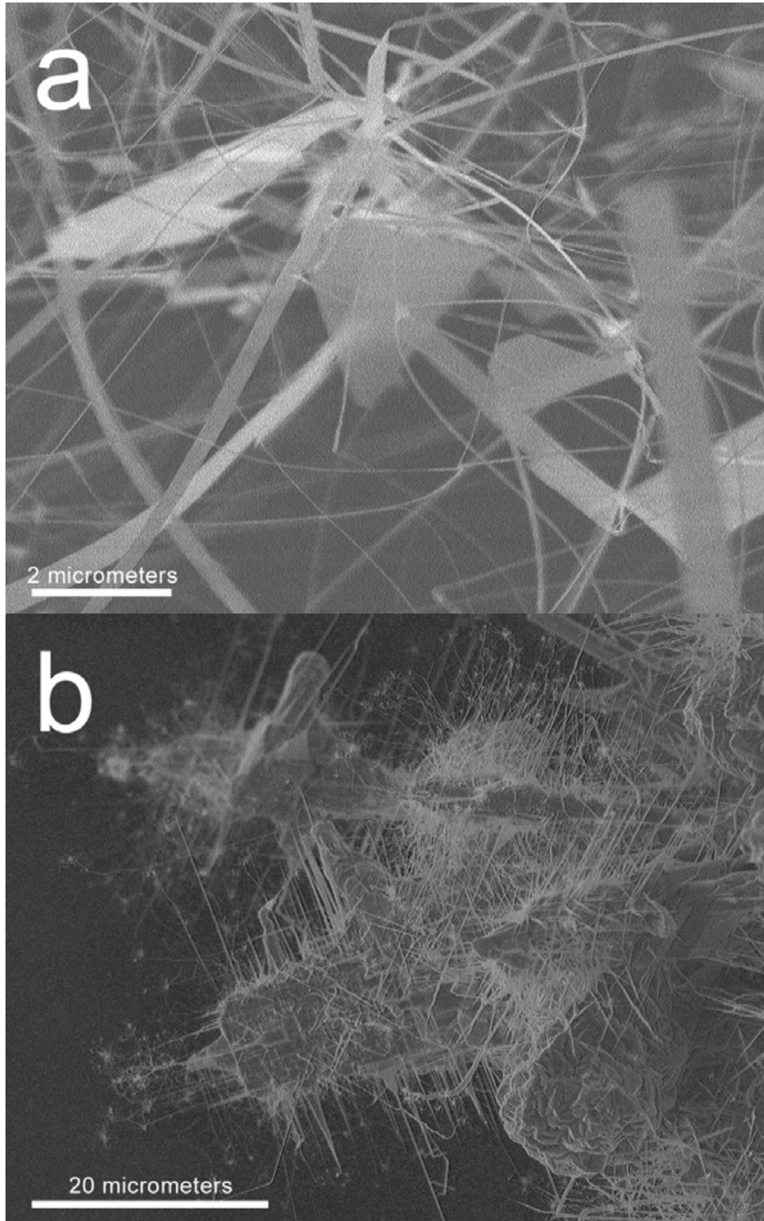

Figure 2

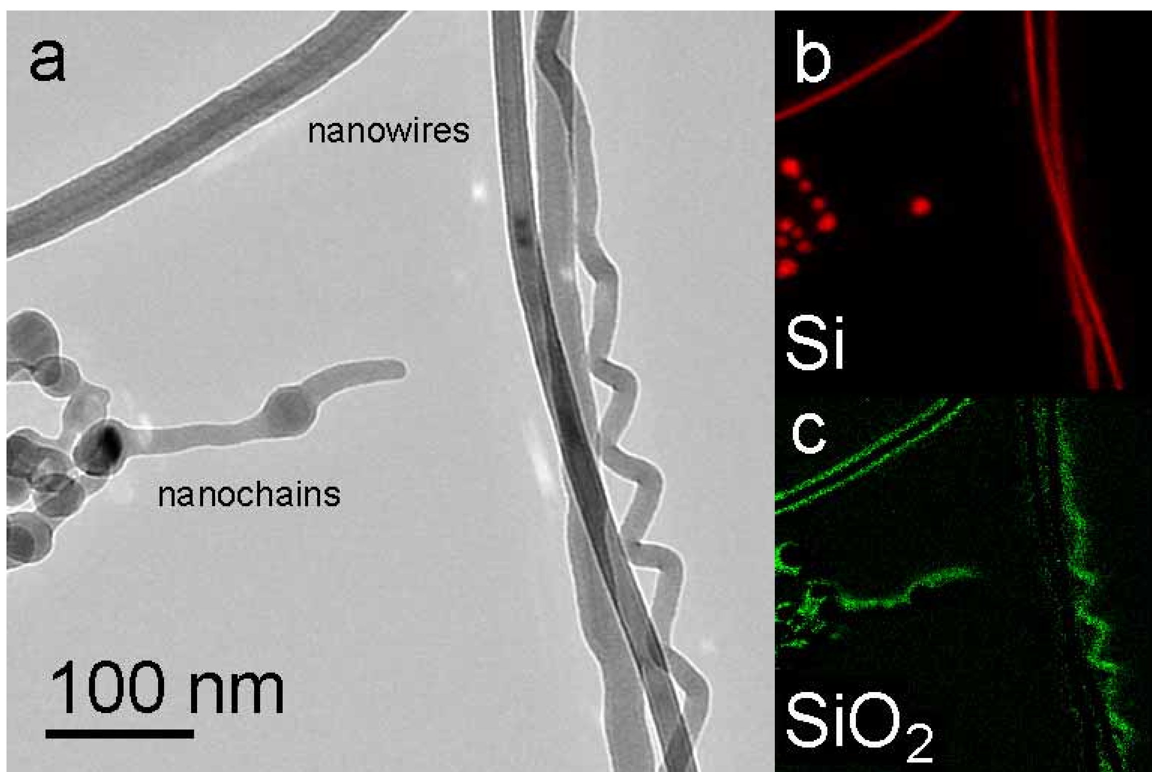

Figure 3

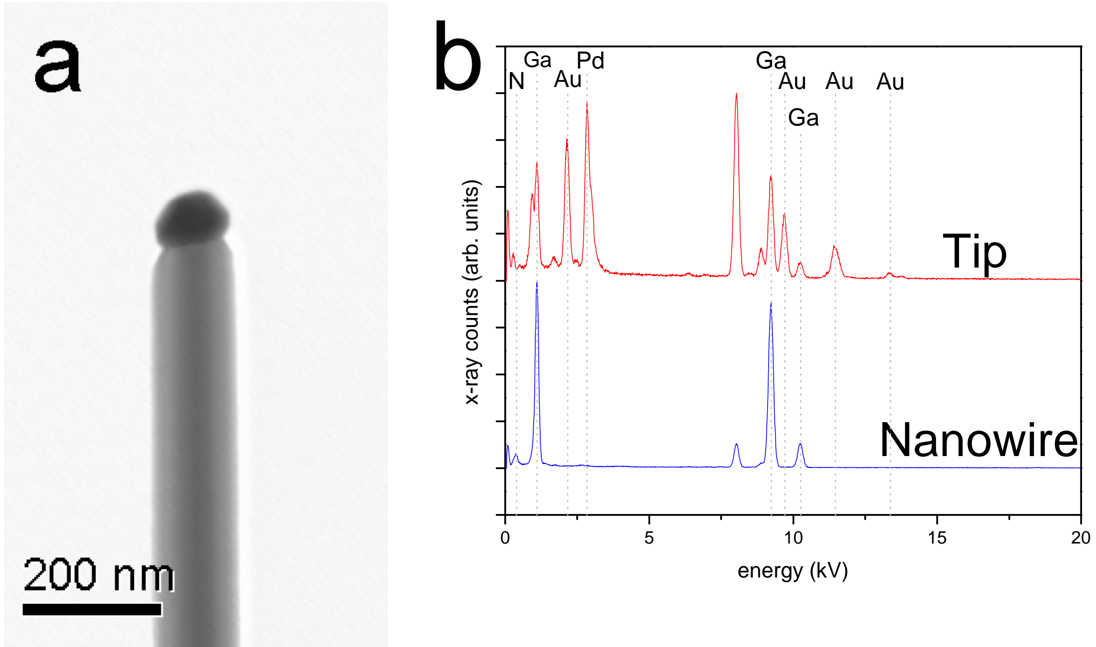

Figure 4

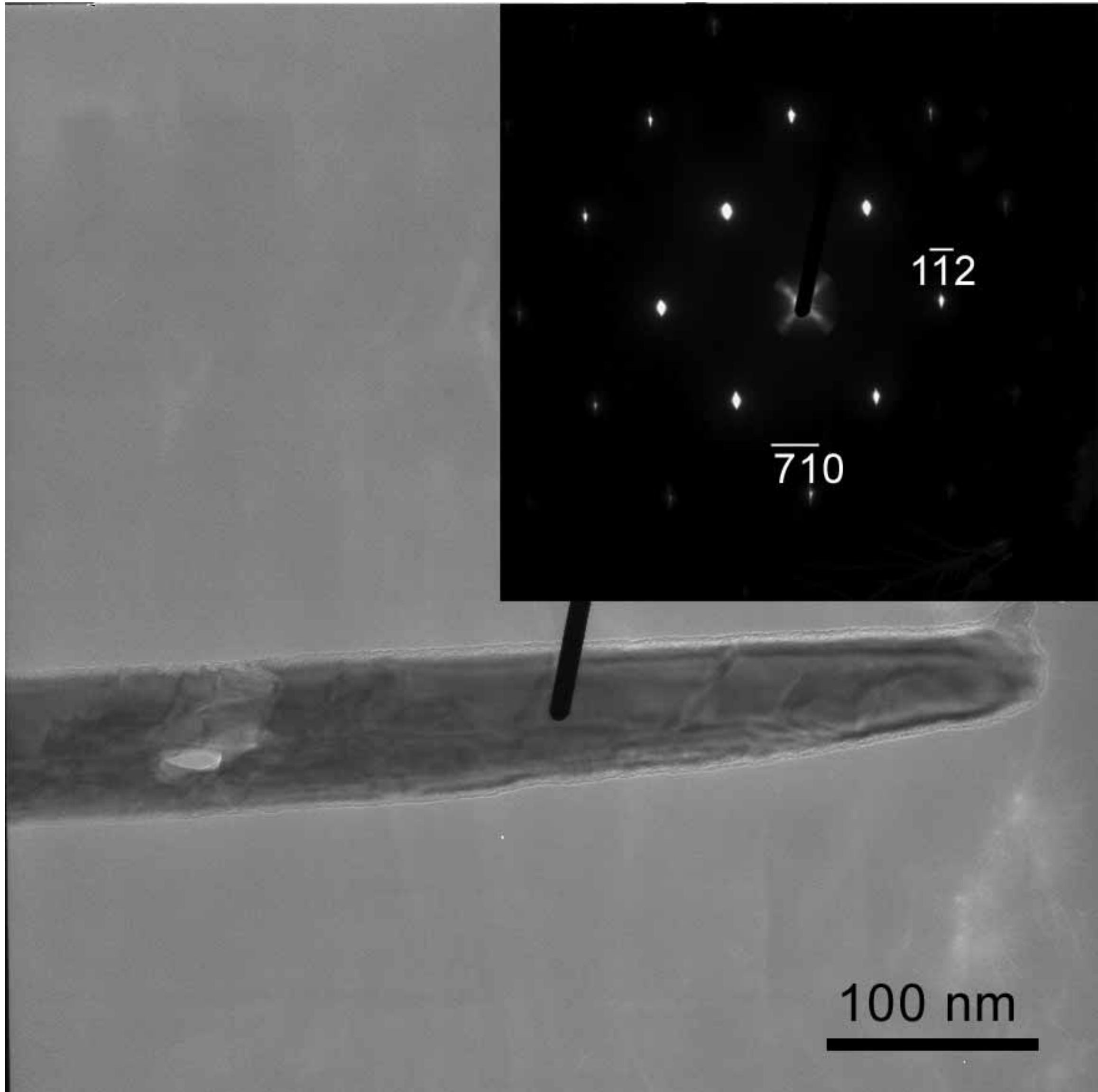

Figure 5

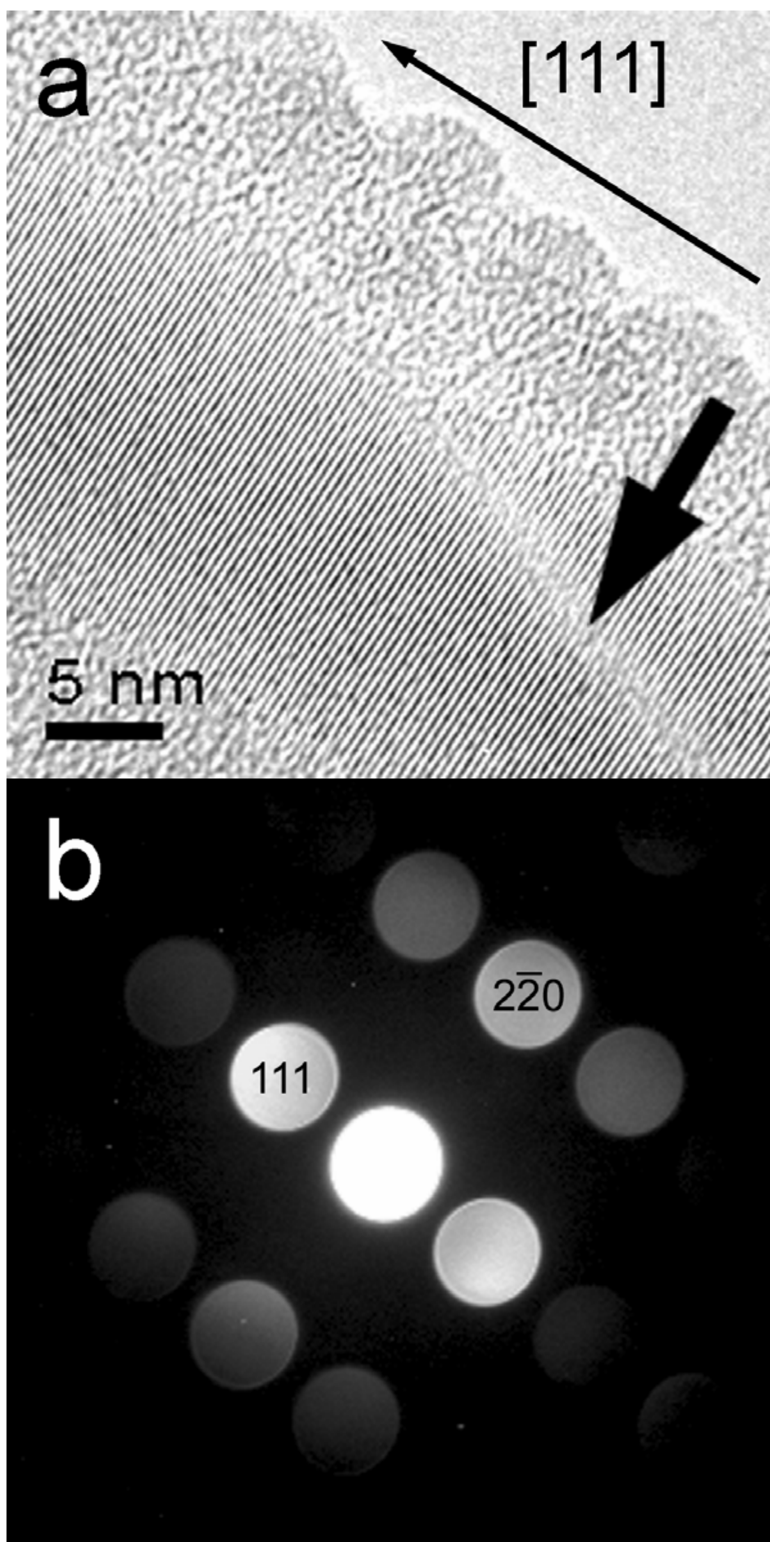

Figure 6